# Blue phosphorene on Au(111) as a decoupling layer for organic epitaxially grown films

Marco Gruenewald, Maximilian Schaal, Iliyan Karadzhov, Lorenz Brill, Jari Domke, Philip Grimm, Felix Otto, Julian Picker,[*] Paul M. Simon, Hendrik Tamm, Torsten Fritz, and Roman Forker[†]

*Institute of Solid State Physics, Friedrich Schiller University Jena, Helmholtzweg 5, 07743 Jena, Germany*

Blue phosphorene (BlueP) is considered as a promising two-dimensional (2D) material for future-(opto)electronic applications. Monolayer BlueP is often fabricated on Au(111) single-crystal surfaces. It has been suggested that small P domains form a lateral network with Au adatoms. Previous studies attempting to use BlueP/Au(111) as a substrate for the deposition of fullerene indicated that the former is susceptible to structural deterioration, unlike most other 2D materials in this regard. Here, we investigate 3,4:9,10-perylenetetracarboxylic dianhydride (PTCDA) monolayers and multilayer films deposited on BlueP/Au(111). We monitor the film growth in real time using *in situ* optical differential reflectance spectroscopy with the substrate kept either at room temperature or at $\approx 120\,°\text{C}$. Furthermore, we examine the epitaxial alignment between PTCDA and BlueP by means of distortion-corrected low-energy electron diffraction and low-temperature scanning tunneling microscopy. Our data clearly reveal that PTCDA exhibits a highly ordered monolayer structure with a herringbone packing motif, whereas the domain orientations differ from all previously reported structures of PTCDA directly on Au(111). Importantly, we find no indications for adsorption-induced reordering or degradation of BlueP/Au(111). At elevated temperatures, PTCDA is observed to form multilayer islands covering only a fraction of the available PTCDA monolayer surface on BlueP/Au(111), and this Stranski-Krastanov growth mode bears similarities to literature results for PTCDA multilayers on pristine coinage metal surfaces.

## I. INTRODUCTION

Two-dimensional (2D) materials beyond graphene are increasingly drawing attention, giving rise to rapid progress in the synthesis and characterization across diverse chemical categories [1]. With numerous elemental compositions reported so far, phosphorus-based 2D materials have recently moved into the focus [2]. Among the known layered allotropes, black phosphorene (BlackP) and blue phosphorene (BlueP) stand out due to promising electronic properties, such as an adjustable band gap or high charge-carrier mobility [2,3]. Those properties may be useful for future applications in sensors, detectors, or other (opto)electronic devices. In particular, the fabrication of BlueP on Au(111) has sparked notable interest in the microscopic structure where some authors proposed a phosphorus monolayer structure without heteroatoms [4–8], whereas other publications claim that Au-linker atoms are incorporated in between small BlueP subunits [9–11]. Notwithstanding this structural debate, it is intriguing to assess the formation of an interface between a BlueP/Au(111) substrate and a molecular adlayer, which can be readily motivated by the semiconducting properties of many organic materials [12]. However, this has rarely

been investigated so far, unlike for graphene, hexagonal boron nitride, or transition-metal dichalcogenides where numerous studies exist [13–18]. In one of the few reports on this topic, the deposition of buckminsterfullerene ($C_{60}$, CAS no.: 99685-96-8) on BlueP/Au(111) was shown to primarily create defects and disordered BlueP domains with little tendency of $C_{60}$ itself to form ordered assemblies [19]. This susceptibility of BlueP/Au(111) to structural damage upon the adsorption of molecules based on $sp^2$-hybridized carbon is distinctly different from most other 2D materials [13–18]. Furthermore, the electronic coupling of an organic monolayer to a metal substrate is often significantly reduced by a 2D interlayer [14,15,17,18]. The role of BlueP also seems to stand out from most other 2D materials in this regard since the interfacial charge transfer with the aforementioned $C_{60}$ was described as remarkable, judging from the observed strong broadening of the lowest unoccupied molecular orbital [19].

Here, we examine 3,4:9,10-perylenetetracarboxylic dianhydride (PTCDA, $C_{24}H_8O_6$, CAS no.: 128-69-8) films adsorbed on BlueP/Au(111). This is a case study using a prototypical molecule which is known for its tendency to form highly ordered layers on a large variety of substrates [13–16,20–26]. Potential applications of PTCDA layers were reported in the literature, e.g., as a template for subsequently deposited layers used as high-$\kappa$ dielectrics [27], as a light absorbing layer in graphene-based phototransistors [28], or as an electron transport layer in perovskite photovoltaic cells [29]. Exploring the properties of heterointerfaces between PTCDA and two-dimensional materials is, therefore,

---

[*]Also at Institute of Physical Chemistry, Friedrich Schiller University Jena, Lessingstraße 10, 07743 Jena, Germany.

[†]roman.forker@uni-jena.de; home page: www.organics.uni-jena.de/

particularly interesting. Noteworthily, it has been reported that the interface between PTCDA and BlackP is governed by charge transfer [30]. In another study, PTCDA was used as a protective coating for BlackP as the latter is known to be unstable under atmospheric conditions [31]. In the light of the above-mentioned structural degradation of BlueP upon molecular adsorption even in ultra-high vacuum (UHV) [19], the structural interplay at the PTCDA/BlueP interface is of special interest to us.

In this paper, we address the questions of: (i) the structural stability of BlueP upon PTCDA adsorption in UHV, (ii) the epitaxial relation formed, (iii) the charged state of the PTCDA adlayer molecules, and (iv) the morphology of PTCDA films of various thicknesses. To this end, we employ a combination of scanning tunneling [hydrogen] microscopy (ST[H]M), distortion-corrected low-energy electron diffraction (LEED), *in situ* optical differential reflectance spectroscopy (DRS), and *ex situ* atomic force microscopy (AFM), among other techniques.

## II. EXPERIMENTAL METHODS

All experiments were performed in UHV with a base pressure in the $10^{-10}$ mbar regime if not stated otherwise. The Au(111) substrate (MaTecK, Jülich, Germany) with a specified purity of 99.999% was cleaned by repeated cycles of sputtering (Ar$^+$, 1 keV, $\approx 4\,\mu\mathrm{A\,cm}^{-2}$) and annealing ($\approx 600\,^\circ$C, 30 min). Phosphorus was deposited by thermal decomposition of InP powder (Sigma-Aldrich) with a specified purity of 99.998% in a water-cooled evaporation source at $550\,^\circ$C whereas the substrate was held at $200\,^\circ$C according to Ref. [5]. The layer formation was monitored *in situ* by means of reflection high-energy electron diffraction (RHEED, EK-35-R electron gun from STAIB Instruments, see the Supplemental Material for further details [32]) using an electron energy of 20 keV. No indium could be detected by means of x-ray photoelectron spectroscopy (XPS) afterwards with the concentration detection threshold being 0.02% with respect to the gold surface.

PTCDA films (Sigma-Aldrich, purified by temperature gradient sublimation [33] and thoroughly degassed in UHV) were deposited from an effusion cell (boron nitride crucible with a shutter) stabilized at $T_{\mathrm{crucible}} = 310\,^\circ$C, resulting in a growth rate of approximately $0.1\,\mathrm{ML\,min}^{-1}$ where "ML" represents a monolayer. The adsorbate layers were examined in reciprocal space by means of LEED (dual-micro-channel plate MCP2-SpectaLEED from Omicron). Geometric distortions and the primary energy error in the raw LEED images were corrected using the software LEEDCAL [34,35]. The corrected and calibrated images were then analyzed with the software LEEDLAB [36] in order to obtain lattice parameters (i.e., the adsorbate lattice vectors $\vec{a}_1$ and $\vec{a}_2$ with the unit-cell angle $\Gamma$) and the epitaxial registry of the PTCDA films with high accuracy (uncertainties $\lesssim 1\%$ are typically achieved). The geometrical relation between the adsorbate and the substrate lattices is expressed by the epitaxy matrix **M** according to Ref. [37],

$$\begin{pmatrix} \vec{a}_1 \\ \vec{a}_2 \end{pmatrix} = \mathbf{M} \cdot \begin{pmatrix} \vec{s}_1 \\ \vec{s}_2 \end{pmatrix} = \begin{pmatrix} M_{11} & M_{12} \\ M_{21} & M_{22} \end{pmatrix} \cdot \begin{pmatrix} \vec{s}_1 \\ \vec{s}_2 \end{pmatrix}. \tag{1}$$

For the unreconstructed Au(111) surface, we use a lattice constant of $|\vec{s}_1| = |\vec{s}_2| = 2.8839$ Å as derived from Ref. [38] and references therein.

During the growth of the PTCDA films, we performed optical DRS. Detailed information about this technique can be found elsewhere [39–41]. Briefly, light from a 100 W halogen lamp operated with a stabilized power supply is focused onto the sample surface, the reflected light is then analyzed by means of a monochromator (SP2156 Acton Research SpectraPro) with a charged-coupled device detector attached (PIXIS:100BR eXcelon/UV from Princeton Instruments). The measured signal is defined as

$$\mathrm{DRS}(E, d) \equiv \frac{\Delta R}{R} := \frac{R(E, d) - R(E, 0)}{R(E, 0)}, \tag{2}$$

with the photon energy $E$, the reflectance $R(E, 0)$ of the pristine substrate, and the reflectance $R(E, d)$ of the substrate on which a film with a thickness $d$ is deposited. Multiple spectra are accumulated during the DRS measurements because the signal of monolayers and even submonolayers of organic thin films is rather small (typical values are $\approx 10^{-3}$ for a monolayer [40]). Therefore, the obtained spectra are the result of averaging multiple spectra within a total accumulation time of 30 s. The layer thicknesses of the PTCDA films were determined by means of DRS where new optical transitions emerge abruptly when molecules start to adsorb in the second or higher monolayers (see Fig. S4 in the Supplemental Material [32]). The corresponding amount of molecules necessary to fully cover the surface with one monolayer of the observed densely packed highly ordered structure is denoted as monolayer equivalent (MLE). This unit is particularly useful when the growth mode is not layer-by-layer so that the amount of deposited material is given as a nominal film thickness.

Scanning tunneling microscopy images were acquired using a commercial apparatus (SPECS JT-LT-STM/AFM with KolibriSensors™) [42]. The atomically resolved image of BlueP was obtained by the so-called scanning tunneling hydrogen microscopy (STHM) technique, introduced by Temirov *et al.* [43]. Briefly, hydrogen is dosed into the UHV chamber (partial pressure $\approx 10^{-7}$ mbar) and partly condenses within the tunneling junction whereas the tip-sample distance is significantly reduced by applying appropriate scanning parameters. As a result, the tunneling current is locally modulated by Pauli repulsion forces with the consequence that the obtained contrast is not only purely electronic, but also topographic to a certain extent. For *ex situ* AFM the commercial device *Nanosurf Easyscan 2 AFM* with standard noncontact silicon cantilevers (resonance frequency: 170 kHz) was operated under ambient conditions.

## III. RESULTS AND DISCUSSION

### A. Structural characterization of BlueP

To begin with, we structurally characterize the BlueP layer that we use later on as a substrate for the growth of PTCDA thin films. The LEED image in Fig. 1(a) clearly reveals the hexagonal BlueP structure (green), which we found in a commensurate (5×5) registry with the substrate (yellow), in accordance with previous studies [6–8,10]. Concomitantly,
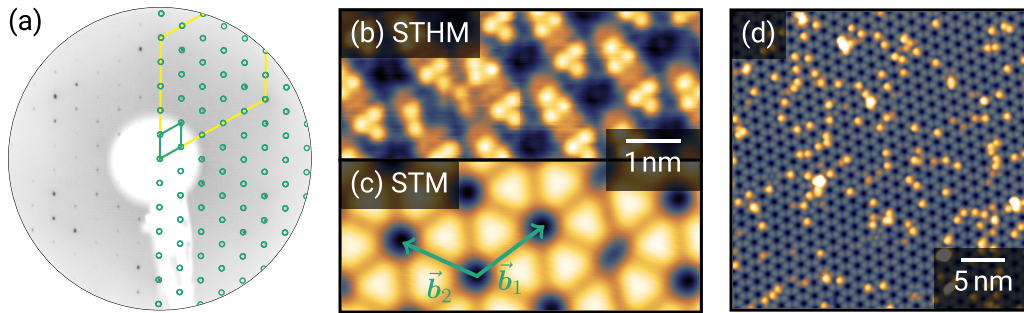
FIG. 1. (a) LEED data of BlueP on Au(111), recorded at an electron energy of 140.0 eV with an inverted contrast of the grayscale image. Half the pattern is superimposed by a fitted lattice simulation where green and yellow circles and lines correspond to BlueP and Au(111), respectively. (b) STHM image ($I = 1\,\mathrm{nA}$, $V = -2\,\mathrm{mV}$, $T = 1.1\,\mathrm{K}$) and (c) STM image ($I = 50\,\mathrm{pA}$, $V = 100\,\mathrm{mV}$, $T = 4.5\,\mathrm{K}$) of BlueP on Au(111). The lattice vectors of the ($5\times5$) structure are depicted in green. (d) Large-scale STM image ($I = 50\,\mathrm{pA}$, $V = 100\,\mathrm{mV}$, $T = 4.5\,\mathrm{K}$) showing the high quality of the BlueP-Au-network on Au(111). The bright protrusions correspond most likely to excess phosphorus clusters adsorbed on BlueP/Au(111) [9].

our *in situ* RHEED data in Fig. S1 in the Supplemental Material corroborate the formation of this ($5\times5$) superstructure during the deposition of phosphorus [32].

The STM image in Fig. 1(c) shows a closeup view of the structure with the previously reported appearance, i.e., dark depressions each surrounded by six bright lobes [4–11]. The specific arrangement of the phosphorus adlayer has been debated in the literature. Earlier experimental realizations were reported in Ref. [4], for example, where only phosphorus atoms were considered in the proposed structural model. Likewise, Zhuang *et al.* interpreted their STM and LEED data with a structural model exclusively consisting of P adatoms [7]. Recently, a new structural model was presented in which a network is formed where BlueP subunits are connected by Au-linker atoms [9–11]. There, the typical BlueP subunits comprise in total nine atoms which arrange in a buckled honeycomb lattice with different adsorption heights of the basis atoms. This arrangement is hardly visible in our conventional STM image in Fig. 1(c). However, in the STHM image in Fig. 1(b), the lateral resolution is significantly improved by the hydrogen-functionalized tunneling junction, making the three topmost P atoms of the BlueP subunits readily visible. The large-area scan in Fig. 1(d) demonstrates the high quality of our BlueP layer, albeit some depressions are occupied, most likely by excess phosphorus clusters [9]. For simplification, we abbreviate the BlueP-Au network with BlueP in the following.

### B. Optical spectroscopy of PTCDA

#### 1. PTCDA films grown at room temperature

PTCDA was deposited onto BlueP/Au(111) with the substrate kept at room temperature (RT). During the deposition, we acquired DRS data which are shown in Fig. 2. In order to quantitatively discuss the optical absorption properties of the molecular film, it is indispensable to extract the optical functions from the measured DRS data for which we used the algorithm described in Ref. [40]. From the obtained complex dielectric function $\varepsilon = \varepsilon' - i\varepsilon''$, the imaginary part $\varepsilon''$ is shown in Fig. 3.

For 1 MLE of PTCDA on BlueP/Au(111) the spectrum in Fig. 3(a) is reminiscent of PTCDA in solution [47–49], albeit

somewhat broadened and redshifted. We conclude that the molecules are essentially in a weakly interacting environment yielding the monomeric behavior of PTCDA. The main peak at 2.30 eV can, thus, be assigned to the fundamental $S_0 \rightarrow S_1$ transition of PTCDA, and the additional peak at $\approx 2.47$ eV can be understood as vibronic replica with an effective vibrational energy of $E_{\mathrm{vib}} \approx 0.17$ eV [47–49]. The optical fingerprint of PTCDA on BlueP/Au(111) differs from that of the PTCDA contact layer directly on the pristine Au(111) surface [45], shown for comparison in Fig. 3(a). The latter spectrum has a rather broad maximum at 2.26 eV, i.e., vibronic features are not observed. This was explained in a previous work [45] by pronounced electronic coupling due to an overlap of substrate states and molecular orbitals, giving rise to a broadening of adsorbate levels according to the Anderson-Newns theory [50,51]. From the observation of a monomerlike spectrum and the absence of any further spectroscopic features, especially any peaks assignable to charged species of PTCDA [24,45,52,53], we conclude that the BlueP layer essentially serves as a decoupling layer for PTCDA. However, in direct comparison with the optical data for PTCDA on mica
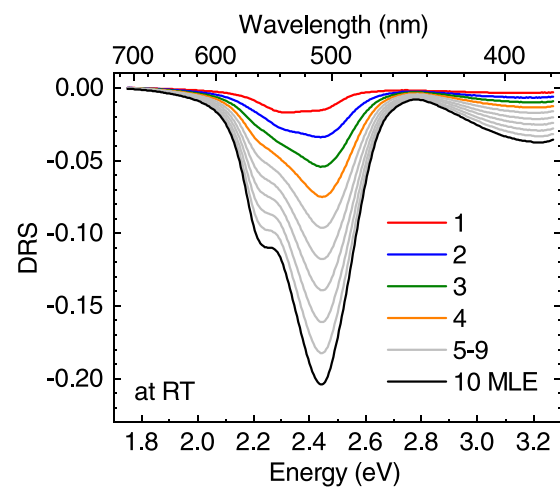


FIG. 2. DRS data of PTCDA on BlueP/Au(111) grown at room temperature. The values in the legend indicate the nominal film thickness $d$ in MLE.
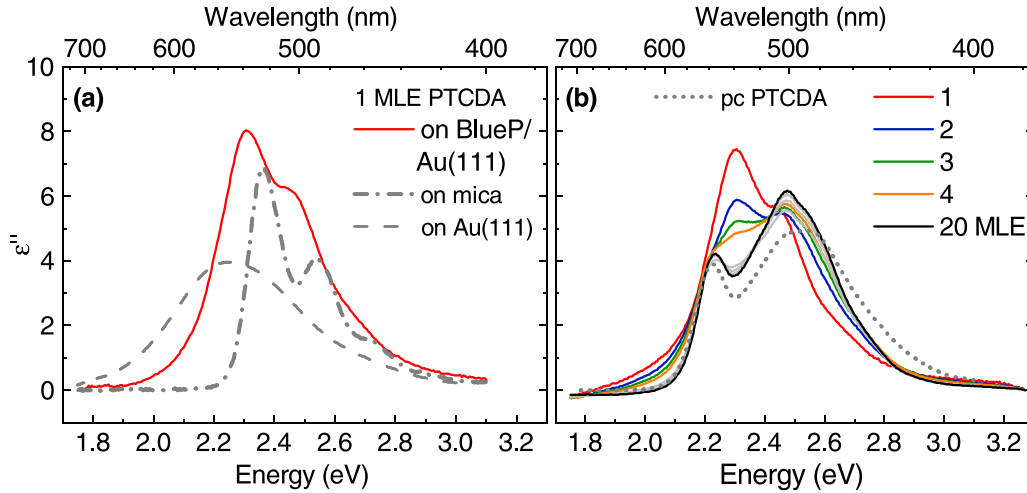
FIG. 3. Imaginary part of the dielectric function $\varepsilon''$ of PTCDA on BlueP/Au(111) grown at room temperature, extracted from the DRS data in Fig. 2 for: (a) 1 MLE and (b) from 1 to 20 MLE. For comparison, $\varepsilon''$ spectra for 1 MLE of PTCDA on mica [44] and directly on pristine Au(111) [45] are shown in (a) and for a relatively thick polycrystalline (pc) film of PTCDA [46] in (b).

in Fig. 3(a), the spectral broadening is somewhat more pronounced. In principal, this can have structural reasons, e.g., inhomogeneous broadening due to molecular disorder, which, however, appears to be moderate from our structural investigation (cf. Sec. III C). We, thus, consider some degree of electronic interaction across the PTCDA/BlueP interface. The optical fingerprints of a ML of PTCDA on different substrates were investigated previously and suggest a hierarchy of the interaction strength [54]. Within this scheme, the spectrum shown here is less broadened than on the bare Au(111) surface but broader than on mica (cf. Fig. 3). Interestingly, we find distinct similarities with the spectrum of a PTCDA ML on graphene/SiC [55] or PTCDA on top of a PTCDA ML pre-deposited on Ag(111) [56] from which we conclude that the electronic interaction between PTCDA and BlueP/Au(111) has a physisorptive character. This statement is corroborated by the XPS measurements shown in Fig. S2 in the Supplemental Material [32] where we do not observe any influence of the adsorption of the PTCDA molecules on the energetic position of the P 2$p$-core levels of BlueP on Au(111). The absence of a significant chemical shift indicates that no covalent bonds between the P and the anhydride groups of PTCDA are formed.

The $\varepsilon''$ spectra of PTCDA submonolayers on BlueP (see Fig. S3 in the Supplemental Material [32]) exhibit almost no deviation from the $d \approx 1$ MLE spectrum; especially the $S_0 \rightarrow S_1$ transition energy remains constant, which was found similarly by some of us for PTCDA on h-BN/Pt(111) [15]. There, we reasoned that the 2D PTCDA domains quickly reach a sufficient size upon coverage increase so that the influence of the lateral aggregation on the optical spectra saturates.

For film thicknesses higher than 1 MLE, the $\varepsilon''$ spectra show a pronounced development: the monomeric features begin to disappear, and the spectral shape broadens with a new shoulder being formed at $\approx 2.23$ eV. This peak can be assigned to a mixing of Frenkel and charge-transfer excitons [57]. The thickness-dependent evolution of our $\varepsilon''$ spectra [see Fig. 3(b)] is very similar to that of PTCDA on Ag(111) with a monolayer of PTCDA predeposited (also at RT) [56], which is indicative of a quasi layer-by-layer growth mode as found

for PTCDA on Ag(111) under similar preparation conditions [58,59].

### 2. PTCDA films grown at elevated temperatures

In order to obtain further insights into the adsorption of PTCDA on BlueP/Au(111) and how an increased surface mobility of the molecules due to additional thermal energy affects the film growth, we recorded *in situ* DRS while keeping the substrate at $\approx 120\,°C$.

In Fig. 4, the DRS data for 1 MLE (red solid line) are similar in shape and energetic position compared to the room-temperature data presented in Fig. 2. However, what is strikingly different is the new behavior of the spectra above 1 MLE: the shape of the main peak gets broader and a much more pronounced peak at $\approx 2.15$ eV becomes dominant and rises gradually in intensity up to 10 MLE. If we extract the dielectric function from these data similarly as we did for the RT data in Fig. 3, we obtain an apparent optical absorption
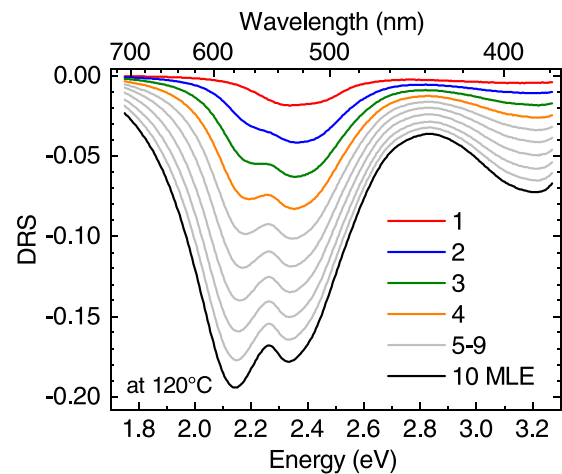


FIG. 4. DRS data of PTCDA on BlueP/Au(111) grown at a substrate temperature of $120\,°C$. The values in the legend indicate the nominal film thickness $d$ in MLE.
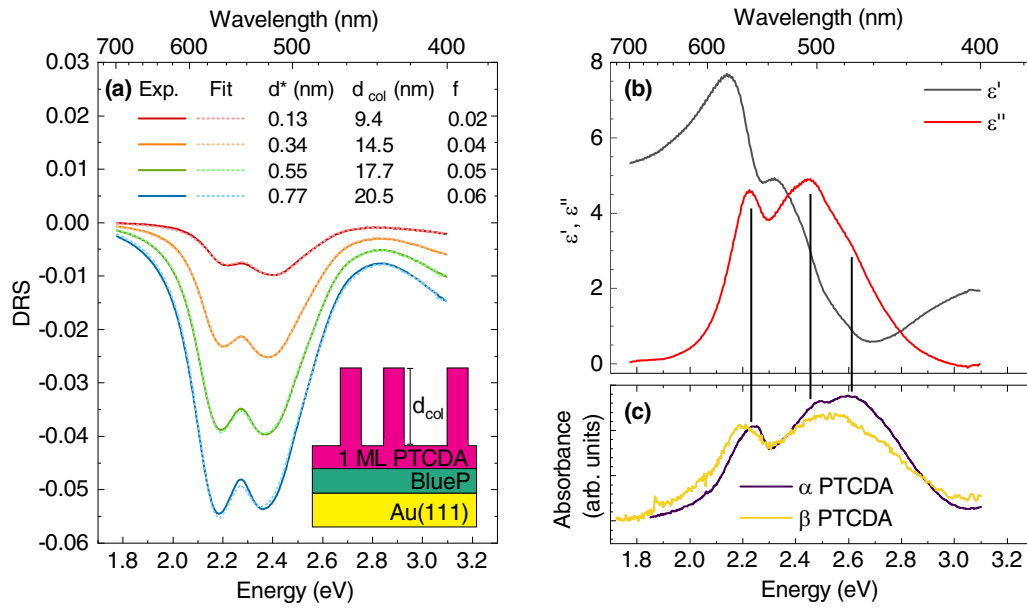
FIG. 5. (a) DRS data of PTCDA grown on BlueP/Au(111) at $\approx 120\,^\circ$C, plotted with the $d = 1$ MLE spectrum as the new reference. All spectra were fitted simultaneously (dotted lines). The proposed growth mode and basis for the fit model is shown in the inset (not to scale) in the bottom right, see the text for details. Furthermore, the thickness $d^*$, the average height of the islands $d_{\mathrm{col}}$ and the areal fraction $f$ are indicated. (b) Optical functions of PTCDA, extracted from the DRS data in Fig. 4. (c) Absorbance of crystalline PTCDA in $\alpha$ and $\beta$ phases (adapted from Ref. [65]). The vertical lines serve as a guide to the eye.

behavior that is very untypical for PTCDA with a dominating peak at $\approx 2.15$ eV (see Fig. S5 in the Supplemental Material [32]). It will be demonstrated in the following that this likely originates from a different morphology of the adsorbate film when grown at elevated temperatures. Experimental verifications of the following assumptions are presented in Fig. S6 in the Supplemental Material [32].

To begin with, we consider the first PTCDA ML to be smooth on BlueP/Au(111), but further deposition leads to the formation of three-dimensional (3D) islands on top, which we assume to have an approximately columnar shape. It is, therefore, reasonable to separate the first ML such that we introduce the *reduced* nominal film thickness $d^* = d - 1$ MLE with $d$ being the *total* nominal film thickness deduced from the deposition rate. In this model, the height of the columns $d_{\mathrm{col}}$ is higher than $d^*$, consequently, parts of the surface (i.e., the PTCDA wetting layer) remain uncovered leading to $d^* = d_{\mathrm{col}} \cdot f$ with the areal fraction $f$ occupied by the PTCDA columns. We further assume that the columns are large enough to optically behave bulklike, i.e., their optical constants are independent from their dimensions. This is justified by the fact that the optical absorption behavior of PTCDA is hardly sensitive to the specific morphology formed, e.g., Han *et al.* presented optical absorption spectra for PTCDA forming nanowires which are very similar to those of PTCDA thin films and $\alpha$-PTCDA single crystals [60]. We fitted the quantity $f \cdot \mathrm{DRS}(E, d_{\mathrm{col}})$ to our experimental data by a pointwise variation of the optical functions of the PTCDA columns (see the Supplemental Material [32]). $d_{\mathrm{col}}$ and $f$ were treated as fit parameters, too. This becomes feasible since we simultaneously fitted multiple spectra where spectral changes only stem from internal interference effects providing information about the vertical dimensions of the columns [61,62]. As a

fitting routine we used the Levenberg-Marquardt algorithm, which is known to be rather robust against different starting values [63,64]. The different spectra were weighted by the factor $1/d^*$ in order to equalize their contributions to the fit. As starting values we used the optical constants of polycrystalline PTCDA [46]. The fit, subsequently, converged into the results shown in Fig. 5.

Our fit results (dashed lines) in Fig. 5(a) agree very well with the experimental data (solid lines) for small nominal thicknesses $d^*$ of up to 0.77 nm. For higher film thicknesses, however, the fit results deviate significantly from the measured spectra (not shown here). We attribute this observation to the ongoing formation of 3D islands likely with a large variety of heights. Our applied film model cannot adequately comply with 3D islands exhibiting different heights and with the fact that their crystal facets have finite slopes as illustrated by Wagner *et al.* for PTCDA on different metal surfaces [66]. Furthermore, our model does not account for scattering effects.

The obtained optical functions $\varepsilon'(E)$ and $\varepsilon''(E)$ are shown in Fig. 5(b) together with literature data for $\alpha$ and $\beta$ PTCDA in (c) [65]. At around 2.23 eV, the extracted $\varepsilon''$ spectrum (red solid line) has a maximum that corresponds to the maximum of the absorbance of PTCDA in the $\alpha$ phase. The peak of the $\varepsilon''$ spectrum at around 2.45 eV and the shoulder at around 2.6 eV also coincide with $\alpha$ PTCDA. From this comparison, it seems that the PTCDA film has formed predominantly in the $\alpha$ phase, but some mixture of $\alpha$ and $\beta$ phases cannot be excluded.

The proposed growth model, according to which initially a wetting layer is formed, followed by island growth, is referred to as the Stranski-Krastanov growth mode in the literature [59,66,67]. For PTCDA on Ag(111), two monolayers
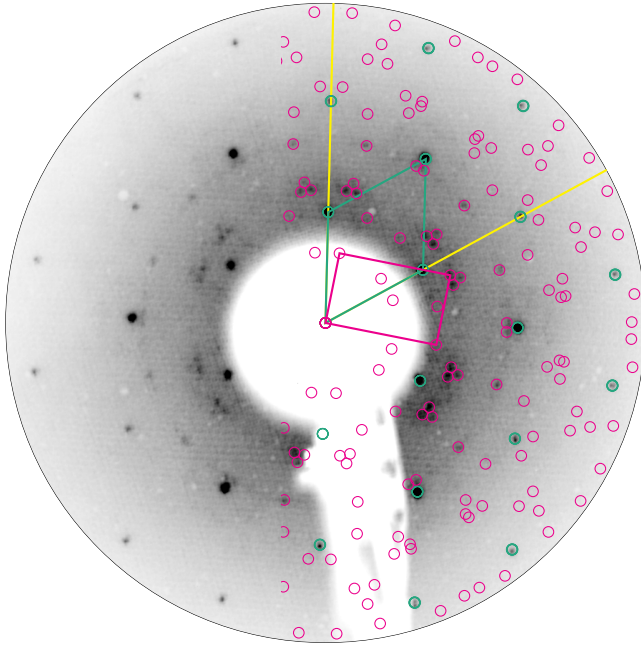
FIG. 6. LEED image of 1 MLE PTCDA on BlueP/Au(111) recorded at an electron energy of 32.8 eV. During the film deposition the substrate was kept at room temperature. The intensity of the grayscale image is inverted. Half of the image is superimposed by a fitted LEED simulation of the PTCDA (magenta, fitting results are summarized in Table I), BlueP (green), and Au(111) (yellow) lattices, respectively.

of PTCDA are initially formed when deposited at substrate temperatures above 320 K [59]. This is similar to our case where also two layers, namely, the BlueP monolayer followed by 1 ML of PTCDA, grow smoothly on Au(111) before a pronounced island growth starts. The formation of 3D PTCDA islands is indicated by the average height of the columns $d_{col}$ and their areal fractions $f$ given in Fig. 5. These values are further supported by our *ex situ* AFM measurements in Fig. S6 in the Supplemental Material showing 3D islands with lateral dimensions in the micrometer range [32].

Our findings are consistent with previous reports, e.g., Krause *et al.* quantitatively examined the temperature depen-

dence of the transition from layer-by-layer growth to island growth for PTCDA on Ag(111) [58].

### C. Lateral structure investigation

The structure of 1 MLE PTCDA on BlueP/Au(111) grown at RT is probed in reciprocal and real space by means of LEED and STM, respectively. After the deposition of 1 MLE of PTCDA, new well-defined diffraction spots arise in addition to the already presented (5×5) superstructure of BlueP on Au(111) in LEED which indicate the growth of highly ordered PTCDA domains. To quantitatively analyze the lateral structure, we fitted a lattice simulation to the observed diffraction spots by taking into account rotational and mirror domains due to the substrate symmetry. The results are visualized in Fig. 6 and summarized in Table I. The structural relation between the PTCDA and the underlying BlueP layer is given by the epitaxy matrix,

$$\mathbf{M}_{LEED} = \begin{pmatrix} 0.75(1) & -0.17(1) \\ 1.00(1) & 1.54(1) \end{pmatrix}. \tag{3}$$

The influence of the BlueP interlayer becomes clearly evident by comparing our structural results with the lateral structure of PTCDA on bare Au(111) [68,69]. Upon depositing PTCDA on Au(111), Kilian *et al.* observed one non-equilibrium structure ($T_{substrate} = 310$ K) and two equilibrium structures ($T_{substrate} = 450$ K) [69]. The reported lattice parameters are shown in Table I, and a graphical comparison in Fig. S7 in the Supplemental Material (including two additional weak structures depicted in Ref. [69]) readily demonstrates that our presented PTCDA structure differs from the reported structures of PTCDA on Au(111) [32]. We conclude that in our case the whole Au(111) surface is covered with BlueP and the latter affects the orientation of the PTCDA domains with respect to the Au(111) substrate. From the good agreement of the lattice dimensions $|\vec{a}_1|$, $|\vec{a}_2|$, and $\Gamma$, it is quite reasonable to assume that PTCDA forms the well-known herringbone structure also on BlueP/Au(111). Furthermore, Table I compares our results to the two known bulk phases of PTCDA [70] and yields that the unit cell of 1 MLE PTCDA on BlueP/Au(111) is closer to $\beta$ than to $\alpha$ PTCDA. We note that our optical results of the PTCDA multilayers suggest that those resemble the $\alpha$ phase (see above). This, however,

TABLE I. The structural parameters of 1 MLE PTCDA on BlueP/Au(111) compared to 1 ML PTCDA directly on Au(111) [69] and the (102) plane of $\alpha$ and $\beta$ PTCDA [70]. $\vec{a}_1$, $\vec{a}_2$: PTCDA lattice vectors; $\Gamma$: unit cell angle between $\vec{a}_1$ and $\vec{a}_2$; $\theta$: PTCDA domain angle between $\vec{a}_1$ and the Au lattice vector $\vec{s}_1$ (which is parallel to the BlueP lattice vector $\vec{b}_1$). Primitive gold lattice vectors enclose an angle of 120°. Numbers in parentheses indicate the uncertainty of the last significant digit.

|  | $|\vec{a}_1|$ (Å) | $|\vec{a}_2|$ (Å) | $\Gamma$ (°) | $\theta$ (°) |
|---|---|---|---|---|
| 1 MLE PTCDA on BlueP/Au(111) via LEED[a] | 12.3(1) | 19.6(2) | 90.4(3) | -10.1(2) |
| 1 MLE PTCDA on BlueP/Au(111) via fast Fourier transform (FFT)[a] | 12.32(6) | 19.30(4) | 90.1(4) | -10.5(2) |
| 1 ML PTCDA directly on Au(111), structure $A$[b] | 12.3(1) | 19.2(1) | 90.0(3) | 7.5(3) |
| 1 ML PTCDA directly on Au(111), structure $B_1$[b] | 12.1(1) | 19.2(1) | 90.0(3) | 39.5(5) |
| 1 ML PTCDA directly on Au(111), structure $B_2$[b] | 12.1(1) | 19.2(1) | 90.0(3) | 37.0(5) |
| Bulk $\alpha$-PTCDA (102) plane[c] | 11.96 | 19.91 | 90 | |
| Bulk $\beta$-PTCDA (102) plane[c] | 12.45 | 19.30 | 90 | |

[a]This paper.
[b]Reference [69].
[c]Reference [70].

does not contradict the PTCDA contact layer resembling the β-PTCDA surface unit cell since LEED is essentially sensitive to the first PTCDA monolayer, which grows smoothly and covers the BlueP surface entirely. On the other hand, the multilayer samples exhibit rather high columns covering less than 10% of the available surface, which is why the first PTCDA monolayer remains dominant in LEED images even for multilayer samples (not shown here). For our DRS measurement, the situation is different since a growing number of deposited molecules means that the DRS signal is more and more dominated by the aggregates forming. For those dominant aggregates (in the multilayer samples) the optical functions closely resemble the α-PTCDA bulk behavior. Similar structural findings were reported by Kilian *et al.* where the unit cell of the first two monolayers of PTCDA on Ag(111) resemble that of the β phase, whereas the multilayer islands on top crystallize in the α phase [67].

The herringbone structure is also verified by the STM measurement in Fig. 7. The PTCDA unit cell is marked by the magenta lattice. On closer inspection of the STM image, one discovers a different orientation of the neighboring molecules (visualized by blue and black arrows along the dashed line) as well as an apparent height variation within the PTCDA domains. These observations suggest the presence of a moiré structure caused by the different lattice parameters of PTCDA and the underlying BlueP interlayer. Please note that these variations in the STM image do not have the same periodicity as the depressions in the BlueP superstructure [cf. Fig. 1(c)], whose lattice vectors are depicted in green in the upper right inset in Fig. 7(a).

To get a detailed analysis of the local lateral structure we computed the FFT of Fig. 7(a). We identified the PTCDA structure (marked as magenta lines and circles) and the underlying BlueP superstructure (marked as green lines) in the FFT and fitted simultaneously a hexagonal and a rectangular lattice with starting values obtained from our LEED measurements. Since we choose an STM image of only one molecular domain, the geometric simulation differs from the LEED analysis displayed in Fig. 6. The additional weak spots visible there can be described geometrically by multiple scattering at both structures (marked as light blue circles). By simultaneous fitting of the PTCDA and BlueP structures, we determined the epitaxy matrix of PTCDA with respect to the BlueP lattice,

$$\mathbf{M}_{\mathrm{FFT}} = \begin{pmatrix} 0.751(2) & -0.179(3) \\ 1.001(3) & 1.520(3) \end{pmatrix}. \qquad (4)$$

Furthermore, by using the known commensurate (5×5) relation between the BlueP and the unreconstructed gold substrate lattices, we determined the lattice parameters of the PTCDA on BlueP (see Table I), which are in very good agreement with the results of our LEED analysis. The eptiaxial registry can be classified as an on-line coincidence of the order $(3,4)_{\mathrm{PTCDA}}{:}(4,0)_{\mathrm{BlueP}}$ [37].

## IV. CONCLUSION

In this paper, we investigated the optical and structural properties of mono- and multilayers of the PTCDA on BlueP/Au(111). By using complementary structural characterization techniques, i.e., LEED and STM, we observed a highly ordered herringbone structure in the first PTCDA
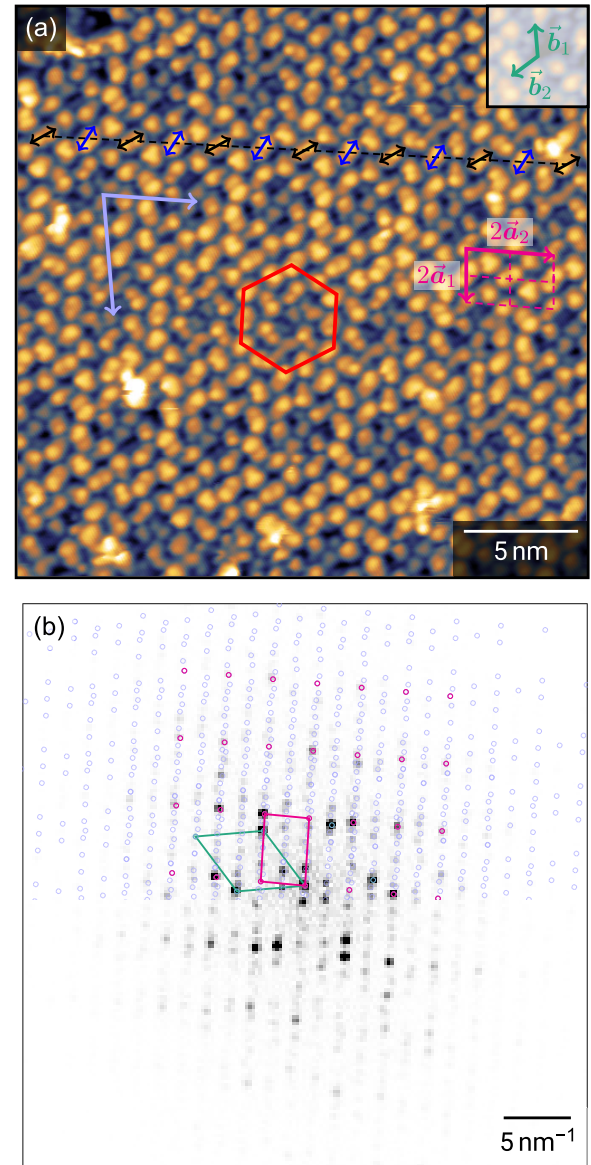


FIG. 7. (a) STM image ($I = 10\,\mathrm{pA}$, $V = 100\,\mathrm{mV}$, $T = 4.5\,\mathrm{K}$) of a PTCDA domain on BlueP/Au(111). The unit cell of the PTCDA herringbone structure is marked with the magenta lattice ($\vec{a}_1$, $\vec{a}_2$). Furthermore, the moiré lattice is marked with light blue vectors. The red hexagon highlights an apparent height variation due to the moiré effect. The inset in the upper right corner shows the lattice vectors $\vec{b}_1$ and $\vec{b}_2$ of the underlying (5×5) BlueP structure. (b) FFT of the STM image in (a). Half of the FFT image is superimposed with a lattice fit of the BlueP superstructure (green, see Fig. 1) and the PTCDA structure (magenta) including multiple scattering with the BlueP structure (light blue circles).

monolayer. Furthermore, we classified the epitaxial registry of the PTCDA as an on-line coincidence of the order $(3,4)_{\mathrm{PTCDA}}{:}(4,0)_{\mathrm{BlueP}}$. In contrast to previous findings in the literature, our LEED and STM data lack any significant indication for a reordering or degradation of the BlueP/Au(111) substrate upon molecular deposition. Our optical measurements of the first PTCDA monolayer showed that, even though the so-called BlueP likely consists of phosphorus

subunits linked via Au adatoms rather than a purely 2D phosphorus layer, it serves as a decoupling layer for the adsorption of this organic molecule. By depositing the PTCDA at elevated temperatures, we observed a pronounced island growth beyond the first smooth monolayer, which results in interference effects within the thick PTCDA columns. The island growth is also confirmed by our *ex situ* AFM measurements. The monolayer unit cell is closer to $\beta$ than to $\alpha$ PTCDA whereas the optical functions of the PTCDA multilayers resemble those of the $\alpha$ phase. A similar structural behavior was found previously for PTCDA mono- and multilayers on Ag(111).

[1] G. R. Bhimanapati, Z. Lin, V. Meunier, Y. Jung, J. Cha, S. Das, D. Xiao, Y. Son, M. S. Strano, V. R. Cooper, L. Liang, S. G. Louie, E. Ringe, W. Zhou, S. S. Kim, R. R. Naik, B. G. Sumpter, H. Terrones, F. Xia, Y. Wang, J. Zhu, D. Akinwande, N. Alem, J. A. Schuller, R. E. Schaak, M. Terrones, and J. A. Robinson, Recent advances in two-dimensional materials beyond graphene, ACS Nano **9**, 11509 (2015).

[2] M. Akhtar, G. Anderson, R. Zhao, A. Alruqi, J. E. Mroczkowska, G. Sumanasekera, and J. B. Jasinski, Recent advances in synthesis, properties, and applications of phosphorene, npj 2D Mater. Appl. **1**, 5 (2017).

[3] H. Liu, A. T. Neal, Z. Zhu, Z. Luo, X. Xu, D. Tománek, and P. D. Ye, Phosphorene: An unexplored 2D semiconductor with a high hole mobility, ACS Nano **8**, 4033 (2014).

[4] J. L. Zhang, S. Zhao, C. Han, Z. Wang, S. Zhong, S. Sun, R. Guo, X. Zhou, C. D. Gu, K. D. Yuan, Z. Li, and W. Chen, Epitaxial growth of single layer blue phosphorus: A new phase of two-dimensional phosphorus, Nano Lett. **16**, 4903 (2016).

[5] J.-P. Xu, J.-Q. Zhang, H. Tian, H. Xu, W. Ho, and M. Xie, One-dimensional phosphorus chain and two-dimensional blue phosphorene grown on Au(111) by molecular-beam epitaxy, Phys. Rev. Materials **1**, 061002(R) (2017).

[6] W. Zhang, H. Enriquez, Y. Tong, A. Bendounan, A. Kara, A. P. Seitsonen, A. J. Mayne, G. Dujardin, and H. Oughaddou, Epitaxial synthesis of blue phosphorene, Small **14**, 1804066 (2018).

[7] J. Zhuang, C. Liu, Q. Gao, Y. Liu, H. Feng, X. Xu, J. Wang, J. Zhao, S. X. Dou, Z. Hu, and Y. Du, Band gap modulated by electronic superlattice in blue phosphorene, ACS Nano **12**, 5059 (2018).

[8] E. Golias, M. Krivenkov, A. Varykhalov, J. Sánchez-Barriga, and O. Rader, Band renormalization of blue phosphorus on Au(111), Nano Lett. **18**, 6672 (2018).

[9] H. Tian, J.-Q. Zhang, W. Ho, J.-P. Xu, B. Xia, Y. Xia, J. Fan, H. Xu, M. Xie, and S. Y. Tong, Two-dimensional metal-phosphorus network, Matter **2**, 111 (2020).

[10] J. L. Zhang, S. Zhao, S. Sun, H. Ding, J. Hu, Y. Li, Q. Xu, X. Yu, M. Telychko, J. Su, C. Gu, Y. Zheng, X. Lian, Z. Ma, R. Guo, J. Lu, Z. Sun, J. Zhu, Z. Li, and W. Chen, Synthesis of monolayer blue phosphorus enabled by silicon intercalation, ACS Nano **14**, 3687 (2020).

[11] S. Zhao, J. L. Zhang, W. Chen, and Z. Li, Structure of blue phosphorus grown on Au(111) surface revisited, J. Phys. Chem. C **124**, 2024 (2020).

[12] C. Wang, H. Dong, L. Jiang, and W. Hu, Organic semiconductor crystals, Chem. Soc. Rev. **47**, 422 (2018).

[13] Q. H. Wang and M. C. Hersam, Room-temperature molecular-resolution characterization of self-assembled organic monolayers on epitaxial graphene, Nat. Chem. **1**, 206 (2009).

[14] H. T. Zhou, J. H. Mao, G. Li, Y. L. Wang, X. L. Feng, S. X. Du, K. Müllen, and H.-J. Gao, Direct imaging of intrinsic molecular orbitals using two-dimensional, epitaxially-grown, nanostructured graphene for study of single molecule and interactions, Appl. Phys. Lett. **99**, 153101 (2011).

[15] R. Forker, T. Dienel, A. Krause, M. Gruenewald, M. Meissner, T. Kirchhuebel, O. Gröning, and T. Fritz, Optical transition energies of isolated molecular monomers and weakly interacting two-dimensional aggregates, Phys. Rev. B **93**, 165426 (2016).

[16] X. Liu, J. Gu, K. Ding, D. Fan, X. Hu, Y.-W. Tseng, Y.-H. Lee, V. Menon, and S. R. Forrest, Photoresponse of an organic semiconductor/two-dimensional transition metal dichalcogenide heterojunction, Nano Lett. **17**, 3176 (2017).

[17] H. Guo, A. J. Martínez-Galera, and J. M. Gómez-Rodríguez, $C_{60}$ self-orientation on hexagonal boron nitride induced by intermolecular coupling, Nanotechnology **32**, 025711 (2021).

[18] M. Schaal, T. Aihara, M. Gruenewald, F. Otto, J. Domke, R. Forker, H. Yoshida, and T. Fritz, Hybridization vs decoupling: influence of an h-BN interlayer on the physical properties of a lander-type molecule on Ni(111), Beilstein J. Nanotechnol. **11**, 1168 (2020).

[19] D. Zhou, N. Si, Q. Tang, B. Jiang, X. Song, H. Huang, M. Zhou, Q. Ji, and T. Niu, Defect generation and surface functionalization on epitaxial blue phosphorene by $C_{60}$ adsorption, J. Phys. Chem. C **123**, 12947 (2019).

[20] M. Willenbockel, D. Lüftner, B. Stadtmüller, G. Koller, C. Kumpf, S. Soubatch, P. Puschnig, M. G. Ramsey, and F. S. Tautz, The interplay between interface structure, energy level alignment and chemical bonding strength at organic-metal interfaces, Phys. Chem. Chem. Phys. **17**, 1530 (2015).

[21] K. A. Cochrane, A. Schiffrin, T. S. Roussy, M. Capsoni, and S. A. Burke, Pronounced polarization-induced energy level shifts at boundaries of organic semiconductor nanostructures, Nat. Commun. **6**, 8312 (2015).

[22] N. Nicoara, J. Méndez, and J. M. Gómez-Rodríguez, Visualizing the interface state of PTCDA on Au(111) by scanning tunneling microscopy, Nanotechnology **27**, 475707 (2016).

[23] C. Zwick, A. Baby, M. Gruenewald, E. Verwüster, O. T. Hofmann, R. Forker, G. Fratesi, G. P. Brivio, E. Zojer, and T. Fritz, Complex Stoichiometry-Dependent reordering of

3,4,9,10-Perylenetetracarboxylic dianhydride on Ag(111) upon K intercalation, ACS Nano **10**, 2365 (2016).

[24] A. Baby, M. Gruenewald, C. Zwick, F. Otto, R. Forker, G. van Straaten, M. Franke, B. Stadtmüller, C. Kumpf, G. P. Brivio, G. Fratesi, T. Fritz, and E. Zojer, Fully atomistic understanding of the electronic and optical properties of a prototypical doped charge-transfer interface, ACS Nano **11**, 10495 (2017).

[25] D. Bellinger, J. Pflaum, C. Brüning, V. Engel, and B. Engels, The electronic character of PTCDA thin films in comparison to other perylene-based organic semi-conductors: *ab initio*-, TD-DFT and semi-empirical computations of the opto-electronic properties of large aggregates, Phys. Chem. Chem. Phys. **19**, 2434 (2017).

[26] K. Stallberg, A. Namgalies, and U. Höfer, Photoluminescence study of the exciton dynamics at PTCDA/noble-metal interfaces, Phys. Rev. B **99**, 125410 (2019).

[27] W. Li, J. Zhou, S. Cai, Z. Yu, J. Zhang, N. Fang, T. Li, Y. Wu, T. Chen, X. Xie, H. Ma, K. Yan, N. Dai, X. Wu, H. Zhao, Z. Wang, D. He, L. Pan, Y. Shi, P. Wang, W. Chen, K. Nagashio, X. Duan, and X. Wang, Uniform and ultrathin high-$\kappa$ gate dielectrics for two-dimensional electronic devices, Nat. Electron. **2**, 563 (2019).

[28] X. Chen, X. Liu, B. Wu, H. Nan, H. Guo, Z. Ni, F. Wang, X. Wang, Y. Shi, and X. Wang, Improving the performance of graphene phototransistors using a heterostructure as the light-absorbing layer, Nano Lett. **17**, 6391 (2017).

[29] S. Tsarev, S. Y. Luchkin, K. J. Stevenson, and P. A. Troshin, Perylenetetracarboxylic dianhydride as organic electron transport layer for n-i-p perovskite solar cells, Synth. Met. **268**, 116497 (2020).

[30] C. Wang, D. Niu, B. Liu, S. Wang, X. Wei, Y. Liu, H. Xie, and Y. Gao, Charge transfer at the PTCDA/Black phosphorus interface, J. Phys. Chem. C **121**, 18084 (2017).

[31] R. Guo, Y. Zheng, Z. Ma, X. Lian, H. Sun, C. Han, H. Ding, Q. Xu, X. Yu, J. Zhu, and W. Chen, Surface passivation of black phosphorus via van der Waals stacked PTCDA, Appl. Surf. Sci. **496**, 143688 (2019).

[32] See Supplemental Material at https://link.aps.org/supplemental/10.1103/PhysRevMaterials.6.015601 for (i) growth monitoring of BlueP on Au(111) by means of RHEED, (ii) XPS measurements of PTCDA on BlueP/Au(111), (iii) submonolayer DRS data of PTCDA on BlueP/Au(111), (iv) determination of $\varepsilon''$ spectra from DRS data, (v) optical microscopy and AFM images of PTCDA on BlueP/Au(111), and (vi) structural comparison to PTCDA directly on Au(111).

[33] A. A. Levin, T. Leisegang, R. Forker, M. Koch, D. C. Meyer, and T. Fritz, Preparation and crystallographic characterization of crystalline modifications of 3,4:9,10-perylenetetracarboxylic dianhydride at room temperature, Cryst. Res. Technol. **45**, 439 (2010).

[34] F. Sojka, M. Meissner, C. Zwick, R. Forker, and T. Fritz, Determination and correction of distortions and systematic errors in low-energy electron diffraction, Rev. Sci. Instrum. **84**, 015111 (2013).

[35] LEEDCal 2013, version 4.0, Falko Sojka and Torsten Fritz, Fritz & Sojka GbR, Apolda Germany (2018).

[36] LEEDLab 2018, version 1.0, Falko Sojka and Torsten Fritz, Fritz & Sojka GbR, Apolda Germany (2018).

[37] R. Forker, M. Meissner, and T. Fritz, Classification of epitaxy in reciprocal and real space: rigid versus flexible lattices, Soft Matter **13**, 1748 (2017).

[38] X.-G. Lu, M. Selleby, and B. Sundman, Assessments of molar volume and thermal expansion for selected bcc, fcc and hcp metallic elements, CALPHAD **29**, 68 (2005).

[39] R. Forker and T. Fritz, Optical differential reflectance spectroscopy of ultrathin epitaxial organic films, Phys. Chem. Chem. Phys. **11**, 2142 (2009).

[40] R. Forker, M. Gruenewald, and T. Fritz, Optical differential reflectance spectroscopy on thin molecular films, Annu. Rep. Prog. Chem., Sect. C: Phys. Chem. **108**, 34 (2012).

[41] H. Zaglmayr, C. G. Hu, L. D. Sun, and P. Zeppenfeld, Optical referencing in differential reflectance spectroscopy, Meas. Sci. Technol. **25**, 115603 (2014).

[42] S. Torbrügge, O. Schaff, and J. Rychen, Application of the KolibriSensor to combined atomic-resolution scanning tunneling microscopy and noncontact atomic-force microscopy imaging, J. Vac. Sci. Technol. B **28**, C4E12 (2010).

[43] R. Temirov, S. Soubatch, O. Neucheva, A. C. Lassise, and F. S. Tautz, A novel method achieving ultra-high geometrical resolution in scanning tunnelling microscopy, New J. Phys. **10**, 053012 (2008).

[44] H. Proehl, R. Nitsche, T. Dienel, K. Leo, and T. Fritz, *In situ* differential reflectance spectroscopy of thin crystalline films of PTCDA on different substrates, Phys. Rev. B **71**, 165207 (2005).

[45] R. Forker, C. Golnik, G. Pizzi, T. Dienel, and T. Fritz, Optical absorption spectra of ultrathin PTCDA films on gold single crystals: Charge transfer beyond the first monolayer, Org. Electron. **10**, 1448 (2009).

[46] A. B. Djurišić, T. Fritz, and K. Leo, Modeling the optical constants of organic thin films: application to 3,4,9,10-perylenetetracarboxylic dianhydride (PTCDA), Opt. Commun. **183**, 123 (2000).

[47] V. Bulović, P. E. Burrows, S. R. Forrest, J. A. Cronin, and M. E. Thompson, Study of localized and extended excitons in 3,4,9,10-perylenetetracarboxylic dianhydride (PTCDA) I. Spectroscopic properties of thin films and solutions, Chem. Phys. **210**, 1 (1996).

[48] K. Gustav, M. Leonhardt, and H. Port, Theoretical investigations on absorption and fluorescence of perylene and its tetracarboxylic derivatives, Monatsh. Chem. **128**, 105 (1997).

[49] U. Gómez, M. Leonhardt, H. Port, and H. C. Wolf, Optical properties of amorphous ultrathin films of perylene derivatives, Chem. Phys. Lett. **268**, 1 (1997).

[50] P. W. Anderson, Localized magnetic states in metals, Phys. Rev. **124**, 41 (1961).

[51] D. M. Newns, Self-consistent model of hydrogen chemisorption, Phys. Rev. **178**, 1123 (1969).

[52] T. Dienel, A. Krause, R. Alle, R. Forker, K. Meerholz, and T. Fritz, Alkali metal doped organic molecules on insulators: charge impact on the optical properties, Adv. Mater. **22**, 4064 (2010).

[53] M. Gruenewald, L. K. Schirra, P. Winget, M. Kozlik, P. F. Ndione, A. K. Sigdel, J. J. Berry, R. Forker, J.-L. Brédas, T. Fritz, and O. L. A. Monti, Integer charge transfer and hybridization at an organic semiconductor/conductive oxide interface, J. Phys. Chem. C **119**, 4865 (2015).

[54] R. Forker, M. Gruenewald, T. Kirchhuebel, and T. Fritz, Recent progress in the consistent interpretation of complementary spectroscopic results obtained on molecular systems, Adv. Opt. Mater. **9**, 2100200 (2021).

[55] M. Meissner, M. Gruenewald, F. Sojka, C. Udhardt, R. Forker, and T. Fritz, Highly ordered growth of PTCDA on epitaxial bilayer graphene, Surf. Sci. **606**, 1709 (2012).

[56] M. Gruenewald, K. Wachter, M. Meissner, M. Kozlik, R. Forker, and T. Fritz, Optical and electronic interaction at metal-organic and organic-organic interfaces of ultra-thin layers of PTCDA and SnPc on noble metal surfaces, Org. Electron. **14**, 2177 (2013).

[57] M. Hoffmann, K. Schmidt, T. Fritz, T. Hasche, V. M. Agranovich, and K. Leo, The lowest energy Frenkel and charge-transfer excitons in quasi-one-dimensional structures: application to MePTCDI and PTCDA crystals, Chem. Phys. **258**, 73 (2000).

[58] B. Krause, F. Schreiber, H. Dosch, A. Pimpinelli, and O. H. Seeck, Temperature dependence of the 2D-3D transition in the growth of PTCDA on Ag(111): A real-time X-ray and kinetic Monte Carlo study, Europhys. Lett. **65**, 372 (2004).

[59] H. Marchetto, T. Schmidt, U. Groh, F. C. Maier, P. L. Lévesque, R. H. Fink, H.-J. Freund, and E. Umbach, Direct observation of epitaxial organic film growth: temperature-dependent growth mechanisms and metastability, Phys. Chem. Chem. Phys. **17**, 29150 (2015).

[60] Y. Han, W. Ning, H. Du, J. Yang, N. Wang, L. Cao, F. Li, F. Zhang, F. Xu, and M. Tian, Preparation, optical and electrical properties of PTCDA nanostructures, Nanoscale **7**, 17116 (2015).

[61] M. Kozlik, S. Paulke, M. Gruenewald, R. Forker, and T. Fritz, Determination of the optical constants of α- and β-zinc(II)-phthalocyanine films, Org. Electron. **13**, 3291 (2012).

[62] M. Kozlik, S. Paulke, M. Gruenewald, R. Forker, and T. Fritz, Optical constants of α- and β-Zinc(II)-Phthalocyanine films, Dataset Papers in Physics **2013**, 926470 (2013).

[63] K. Levenberg, A method for the solution of certain problems in least squares, Quart. Appl. Math. **2**, 164 (1944).

[64] D. W. Marquardt, An algorithm for least-squares estimation of nonlinear parameters, J. Soc. Indust. Appl. Math. **11**, 431 (1963).

[65] M. Leonhardt, O. Mager, and H. Port, Two-component optical spectra in thin PTCDA films due to the coexistence of α- and β-phase, Chem. Phys. Lett. **313**, 24 (1999).

[66] T. Wagner, A. Bannani, C. Bobisch, H. Karacuban, M. Stöhr, M. Gabriel, and R. Möller, Growth of 3,4,9,10-perylenetetracarboxylic-dianhydride crystallites on noble metal surfaces, Org. Electron. **5**, 35 (2004).

[67] L. Kilian, E. Umbach, and M. Sokolowski, Molecular beam epitaxy of organic films investigated by high resolution low energy electron diffraction (SPA-LEED): 3,4,9,10-perylenetetracarboxylicacid-dianhydride (PTCDA) on Ag(111), Surf. Sci. **573**, 359 (2004).

[68] S. Mannsfeld, M. Toerker, T. Schmitz-Hübsch, F. Sellam, T. Fritz, and K. Leo, Combined LEED and STM study of PTCDA growth on reconstructed Au(111) and Au(100) single crystals, Org. Electron. **2**, 121 (2001).

[69] L. Kilian, E. Umbach, and M. Sokolowski, A refined structural analysis of the PTCDA monolayer on the reconstructed Au(111) surface – "Rigid or distorted carpet?", Surf. Sci. **600**, 2633 (2006).

[70] M. Möbus, N. Karl, and T. Kobayashi, Structure of perylene-tetracarboxylic-dianhydride thin films on alkali halide crystal substrates, J. Cryst. Growth **116**, 495 (1992).